Available online at www.sciencedirect.com
SCIENCE DIRECT®
Journal of Solid State Chemistry 177 (2004) 4305–4315
JOURNAL OF SOLID STATE CHEMISTRY
www.elsevier.com/locate/jssc

Ordered perovskites in the $A^{2+}(Li_{1/4}Nb_{3/4})O_3$–$A^{2+}(Li_{2/5}W_{3/5})O_3$ (A^{2+} = Sr, Ca) systems

Hui Wu, Peter K. Davies*

Department of Materials Science and Engineering, The University of Pennsylvania, 3231 Walnut St., Philadelphia, PA 19104-6272, USA

Received 21 July 2004; received in revised form 30 August 2004; accepted 31 August 2004

Abstract

Single-phase 1:2 *B*-site ordered perovskites are formed in the $(1-x)A^{2+}(Li_{1/4}Nb_{3/4})O_3$–$(x)A^{2+}(Li_{2/5}W_{3/5})O_3$ systems, A^{2+} = Sr and Ca, within the range $0.238 \leqslant x \leqslant 0.333$. The X-ray and electron diffraction patterns are consistent with a $P2_1/c$ monoclinic supercell, $a = \sqrt{6}a_c$, $b = \sqrt{2}a_c$, $c = 3\sqrt{2}a_c$, $\beta \approx 125°$, where the 1:2 order is combined with $b^-b^-c^+$ octahedral tilting. Rietveld refinements of the ordered $A(B^{I}_{1/3}B^{II}_{2/3})O_3$ structures give a good fit to a model with B^{I} occupied by Li and Nb, B^{II} by W and Nb, and a general stoichiometry $(Sr,Ca)(Li_{3/4+y/2}Nb_{1/4-y/2})_{1/3}(Nb_{1-y}W_y)_{2/3}O_3$, $y = 0.9x = 0.21-0.30$. The Sr system also includes regions of stability of a 1:3 ordered phase for $0.0 \leqslant x \leqslant 0.111$, and a 1:1 ordered double perovskite for $0.833 \leqslant x \leqslant 1.0$. The formation of the non-stoichiometric 1:2 ordered phases is associated with the large site charge/size differences that can be accessed in these systems, and restricted by local charge imbalances at the *A*-sites for W-rich compositions. These concepts are used to generate stability maps to rationalize the formation of the known 1:2 ordered oxide perovskites.

Keywords: Perovskites; Cation order; Octahedral tilting; Non-stoichiometry; Tungstates; Niobates; Rietveld refinement

1. Introduction

The $Ba(Zn_{1/3}Ta_{2/3})O_3$ family of ordered complex perovskites have been extensively studied due to their outstanding dielectric properties in the microwave region [1–4]. The dielectric response of these systems is strongly influenced by the degree of cation order on the octahedral sites of the perovskite structure; the lowest dielectric losses (highest *Q* values) are observed when the cations adopt an ordered cation arrangement with a "1:2" {ZnTaTa} layered repeat along (111) planes of the perovskite sub-cell. Although most of the known examples of this structure type were restricted to the $A(B^{2+}_{1/3}B^{5+}_{2/3})O_3$ systems (with A = Ba, Sr, Ca; B^{2+} = Sr, Ca, Mg, Mn, Co, Ni, Zn; B^{5+} = Nb, Ta), new examples have been identified with the general stoichiometries, $A(B^{+}_{1/3}B^{4+}_{2/3})O_3$ (A = La; B^+ = Li, B^{4+} = Ti) and $A(B^{+}_{1/3}B^{5+}_{2/3})O_3$ (A = (Sr, Ca)$_{2/3}$La$_{1/3}$; B^+ = Li; B^{5+} = Nb, Ta) [5–7]. For the $A(B^{2+}_{1/3}B^{5+}_{2/3})O_3$ family, the ordered structure is rigidly stoichiometric and it is well known that small levels of additives induce a transformation to a non-stoichiometric, 1:1 ordered double perovskite, or to a fully disordered *B*-site arrangement [4,8–14]. Therefore, the recent discovery of a series of non-stoichiometric 1:2 ordered perovskites in the $(1-x)Ba(Li_{1/4}Nb_{3/4})O_3$–$(x)Ba(Li_{2/5}W_{3/5})O_3$ solid solution system was quite unexpected [15]. This paper examines the formation of similar phases in the $(1-x)Sr(Li_{1/4}Nb_{3/4})O_3$–$xSr(Li_{2/5}W_{3/5})O_3$ and $(1-x)Ca(Li_{1/4}Nb_{3/4})O_3$–$Ca(Li_{2/5}W_{3/5})O_3$ systems.

In the $(1-x)Ba(Li_{1/4}Nb_{3/4})O_3$–$(x)Ba(Li_{2/5}W_{3/5})O_3$ (BLNW) system both end members adopt a hexagonal perovskite structure; however, cubic perovskites are stable for the majority of their solid solutions ($0.238 \leqslant x \leqslant 0.833$) [15]. For $0.238 \leqslant x \leqslant 0.385$, the compositions form a single-phase, 1:2 *B*-site ordered structure ($P\bar{3}m1$, $a \approx \sqrt{2}a_c$, $c \approx \sqrt{3}a_c$). In this range,

*Corresponding author. Fax: +1-215-573-2128.
E-mail address: davies@lrsm.upenn.edu (P.K. Davies).

0022-4596/$ - see front matter © 2004 Elsevier Inc. All rights reserved.
doi:10.1016/j.jssc.2004.08.041

the solid solutions do not include any composition with a 1:2 cation stoichiometry and the two ordered positions in the $A(B^{I}_{1/3}B^{II}_{2/3})O_3$ structure exhibit extensive non-stoichiometry, with B^{I} occupied by Li and Nb, and B^{II} by W and Nb according to the general formula: $Ba[(Li_{3/4+y/2}Nb_{1/4-y/2})_{1/3}(Nb_{1-y}W_y)_{2/3}]O_3$ with $y = 0.21-0.35$ (where $y = 0.9x$). The stabilization of the ordered structures was rationalized in terms of the large site size/charge differences of the B^{I} and B^{II} sites that can be realized in this system; the limitations on the stability of the W-rich compositions was explained by considering the imbalance in the anion bond valences in W–O–W linkages, and the local charge imbalance at the A-site positions.

The present study focuses on the phase stabilities in the $(1-x)A^{2+}(Li_{1/4}Nb_{3/4})O_3$–$(x)A^{2+}(Li_{2/5}W_{3/5})O_3$ systems where A^{2+} = Sr and Ca. In contrast to $Ba(Li_{1/4}Nb_{3/4})O_3$, $Sr(Li_{1/4}Nb_{3/4})O_3$ and $Ca(Li_{1/4}Nb_{3/4})O_3$, both form a cubic perovskite structure [16]. Although the first reports of these compounds indicated the B-site cations were disordered [17], recent investigations of $Sr(Li_{1/4}Nb_{3/4})O_3$ found evidence for two types of 1:3 ordered B-site arrangements that interconvert at approximately 1350 °C [16]. The $Sr(Li_{2/5}W_{3/5})O_3$ end member adopts a 1:1 double perovskite structure with $a = 7.958$ Å [18], while $Ca(Li_{2/5}W_{3/5})O_3$ cannot be stabilized in a perovskite structure and forms a multi-phase mixture. The phase behavior of both systems was investigated using X-ray diffraction, Raman spectroscopy and electron diffraction; Rietveld refinements of selected compositions were conducted on data collected by powder neutron diffraction, and the dielectric properties of ceramic samples were studied at microwave frequencies.

2. Experimental

Samples in the $(1-x)Sr(Li_{1/4}Nb_{3/4})O_3$–$(x)Sr(Li_{2/5}W_{3/5})O_3$ and $(1-x)Ca(Li_{1/4}Nb_{3/4})O_3$–$(x)Ca(Li_{2/5}W_{3/5})O_3$ systems were prepared with $x = 0$, 0.111, 0.238, 0.333, 0.385, 0.556, 0.833, and 1.0 by standard solid-state methods. Stoichiometric amounts of $SrCO_3$ (Cerac, 99.9%) or $CaC_2O_4 \cdot H_2O$ (Alfa Aesar, 99%), Nb_2O_5 (Cerac, 99.95%), Li_2CO_3 (Alfa Aesar, 99.0%), and WO_3 (K&K Laboratories, 99.5%) were mixed and calcined at 700 °C to expel CO_2. For the Sr system after ball milling, the mixtures were pressed into pellets, covered with sacrificial powder of the same composition, and sealed in Pt envelops to avoid the loss of Li. Weighing the pellets before and after reaction monitored the effectiveness of this method in inhibiting volatilization of the components. Equilibrated samples, as gauged by the absence of any changes in the X-ray patterns after additional heating, could be obtained in the range 1300–1350 °C. Sintered pellets were prepared at 1450 °C from powders pressed isostatically at 80,000 psi. For the Ca system the powders were calcined at 600 °C, followed by annealing at 700 °C for 10 h, and could be sintered to high density after an 8 h heat at 1100–1150 °C in Pt envelops filled with sacrificial powder.

X-ray diffraction patterns were collected with a Rigaku diffractometer using a Cu$K\alpha$ source operated at 45 kV and 30 mA. The unit cell parameters were refined by a least-squares procedure using data collected at slow scan speed ($0.2^\circ\,min^{-1}$) and a step size of 0.02°. For Rietveld refinement of the X-ray patterns, a Scintag PAD X diffractometer was used to measure the powder patterns for values of 2θ from 5° to 120° in 0.02° steps with a counting time of 12 s for each step. Data processing was carried out using the GSAS package [19]. TEM analysis was performed with a Philips 420 EM operating at 120 kV. Samples for transmission electron microscopy were prepared by disaggregating the ceramics followed by grinding under acetone in an agate mortar. The powder was then suspended in acetone and dispersed onto a lacey carbon 400 mesh TEM grid. Raman data were collected on the polished pellet surfaces with a Renishaw micro-Raman spectrometer (1 μm beam spot) using a 514.4 nm (2.41 eV) laser line.

Neutron powder diffraction data were collected under ambient conditions using the BT-1 32 detector neutron powder diffractometer at the NIST Center for Neutron Research. A Cu(311) monochromator with a 90° takeoff angle, $\lambda = 1.5404(2)$ Å, and an in-pile collimation of 15 min of arc were used. The sample for neutron powder diffraction was loaded in a vanadium cylinder container. Data were collected over the range 3–165° 2θ with a step size of 0.05°. The Rietveld structural refinement was conducted using the GSAS package [19].

The relative permittivity of the samples, ε_r, was measured from 100 Hz to 1 MHz by the parallel-plate method using an HP 4284A precision LCR meter and a Delta 9920 environment chamber from −150 to 200 °C. Measurements of the dielectric loss, $Q = 1/\tan\delta$, and the temperature coefficient of resonant frequency, τ_f, at microwave frequencies were made using cavity methods. To separate the $TE_{01\delta}$ resonance mode from the higher resonance modes, the samples had an aspect ratio (thickness and diameter of samples) close to 0.45. The temperature coefficient of the resonant frequency (τ_f) was calculated from data collected at 25–75 °C.

3. Results

3.1. $(1-x)Sr(Li_{1/4}Nb_{3/4})O_3$–$(x)Sr(Li_{2/5}W_{3/5})O_3$

X-ray patterns collected from samples across the $(1-x)Sr(Li_{1/4}Nb_{3/4})O_3$–$(x)Sr(Li_{2/5}W_{3/5})O_3$ (SLN–SLW or SNLW) solid solution system are shown in Fig. 1. The pattern for the $Sr(Li_{1/4}Nb_{3/4})O_3$ end member was

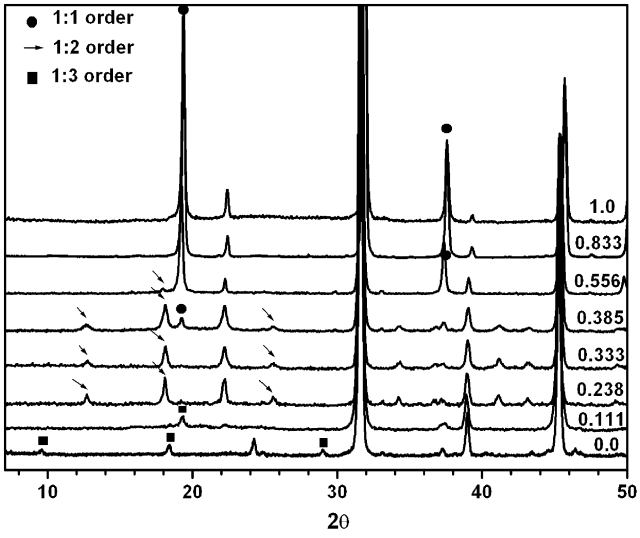

Fig. 1. XRD patterns of $(1-x)Sr(Li_{1/4}Nb_{3/4})O_3$–$xSr(Li_{2/5}W_{3/5})O_3$ with $x = 0.111$, 0.238, 0.333, 0.385, 0.556, 0.833, and 1.00. Superstructure reflections from 1:3 *B*-site order are indicated by squares, 1:2 order by arrows, 1:1 order by circles.

collected from a sample annealed and quenched from 1350 °C. The additional reflections in the X-ray pattern of this sample are identical to those reported for the so-called HT modification of $Sr(Li_{1/4}Nb_{3/4})O_3$ with a $C2/m$ monoclinic cell and $a = 9.815$ Å, $b = 5.665$ Å, $c = 11.333$ Å, $\beta = 125.30°$ [16]. In this ordered form the Li and Nb cations adopt a 1:3 layered arrangement along (111) and the supercell has $a = a_c\sqrt{6}$, $b = a_c\sqrt{2}$, $c = a_c2\sqrt{2}$. As discussed in Ref. [16], the structure converts to a different type of order (LT phase) at ~1325 °C and to a disordered perovskite at ~1420 °C. For $x = 0.111$ the patterns contain very weak and diffuse additional reflections in positions similar to those observed for the $x = 0$ end member and could be indexed in the same monoclinic cell with $a = 9.80(1)$ Å, $b = 5.68(2)$ Å, $c = 11.33(2)$ Å, $\beta = 125.2(1)°$. A series of quenching experiments revealed this composition converts to a disordered structure *B*-site arrangement above 1350 °C.

For the specimens with $0.238 \leqslant x \leqslant 0.333$, the X-ray patterns contained a new set of strong additional reflections in positions (e.g., $2\theta \approx 12°$ and $\approx 18°$) consistent with the formation of a structure with 1:2 ordering of the *B*-site cations. Although most of these reflections could be indexed in the $P\bar{3}m1$ cell with $a = \sqrt{2}a_c$ and $c = \sqrt{3}a_c$, used to index the corresponding 1:2 ordered structures in the BLNW system, several extra split peaks remained unindexed. Complete indexing could be achieved using a monoclinic unit cell with $a = \sqrt{6}a_c$, $b = \sqrt{2}a_c$, $c = 3\sqrt{2}a_c$, $\beta \approx 125°$ which has been used previously to index 1:2 ordered perovskites that exhibit significant octahedral tilting [20]. The appearance of octahedra tilting was not unexpected given the lower tolerance factor of the SNLW compositions (~0.97) compared to their BNLW counterparts (~1.03). The refined lattice parameters yielded $a = 9.787(3)$ Å, $b = 5.647(4)$ Å, $c = 16.967(4)$ Å, $\beta \approx 124.86(1)°$ for $x = 0.238$, and $a = 9.792(1)$ Å, $b = 5.629(5)$ Å, $c = 17.023(3)$ Å, $\beta \approx 125.31(1)°$ for $x = 0.333$.

For $x = 0.385$ and 0.556 superstructure reflections from 1:2 and 1:1 order were visible, with the volume fraction of the 1:2 phase being higher in the former and the 1:1 phase higher in the latter. At $x = 0.833$ the patterns comprised a single set of very strong superlattice reflections originating from the 1:1 ordered phase, and were similar to those of the $Sr(Li_{2/5}W_{3/5})O_3$ end member (see $x = 1.0$ in Fig. 1).

The existence and symmetry of the 1:2 ordered phases was examined in more detail using electron diffraction. A typical set of selected area diffraction patterns from $x = 0.333$ is shown in Fig. 2. In the patterns collected along $[0\bar{1}1]_c$ (Fig. 2a) and $[111]_c$ (Fig. 2b), ordering reflections were clearly visible at $\mathbf{k} = 1/3[111]^*_c$. Additional reflections at $\mathbf{k} = 1/2[111]^*_c$ and $\mathbf{k} = \pm 1/2[1\bar{1}0]^*_c$ were consistent with $b^-b^-c^+$ ($CaTiO_3$-type)-type octahedral tilting which has been observed in other closely related 1:2 ordered perovskite phases [20]. The symmetry of the monoclinic, tilted structure, where $a_m = [\bar{1}\bar{1}2]_c = \sqrt{6}a_c$, $b_m = [1\bar{1}0]_c = \sqrt{2}a_c$, $c_m = 3[110]_c = 3\sqrt{2}a_c$ and $\beta \approx 125°$, can be described in either the $P2_1/c$ or $P2_1/a$ space group; the experimentally observed extinctions were consistent with $P2_1/c$ symmetry.

The ordered phases were also examined using Raman spectroscopy. Previous factor-group analysis of perovskites with a combination of cation ordering and $b^-b^-c^+$ octahedral tilting, predict 24 Raman active modes $(12A_g + 12B_g)$ for 1:1 type order, and 84 Raman active modes $(42A_g + 42B_g)$ for 1:2 ordering [21]. While only some of these modes are observed experimentally (Fig. 3), the peaks near 800 cm^{-1} are particularly sensitive in discriminating between 1:1 (one band at 813 cm^{-1}) and 1:2 (two bands at ~820 and ~860 cm^{-1}) ordering [22].

The stabilization of 1:2 *B*-site order in the SNLW solid solutions is similar to the behavior of the BNLW system, where the non-stoichiometric order arises from the ordering of Li and W on the B^I and B^{II} sites in the $A(B^I_{1/3}B^{II}_{2/3})O_3$ structure and the Nb cations are distributed on both positions according to the general formula $A[(Li_{3/4+y/2}Nb_{1/4-y/2})_{1/3}(Nb_{1-y}W_y)_{2/3}]O_3$ (where $y = 0.9x$). This cation distribution was used as a starting model for Rietveld refinements of neutron diffraction data collected from the $x = 0.333$ sample, where the "ideal" ordered stoichiometry would be $Sr[(Li_{0.9}Nb_{0.1})_{1/3}(Nb_{0.7}W_{0.3})_{2/3}]O_3$. The initial result of the refinement showed only the $P2_1/c$ model with $CaTiO_3$-type ($b^-b^-c^+$) octahedral tilting could fit all of the observed peaks in the neutron diffraction patterns.

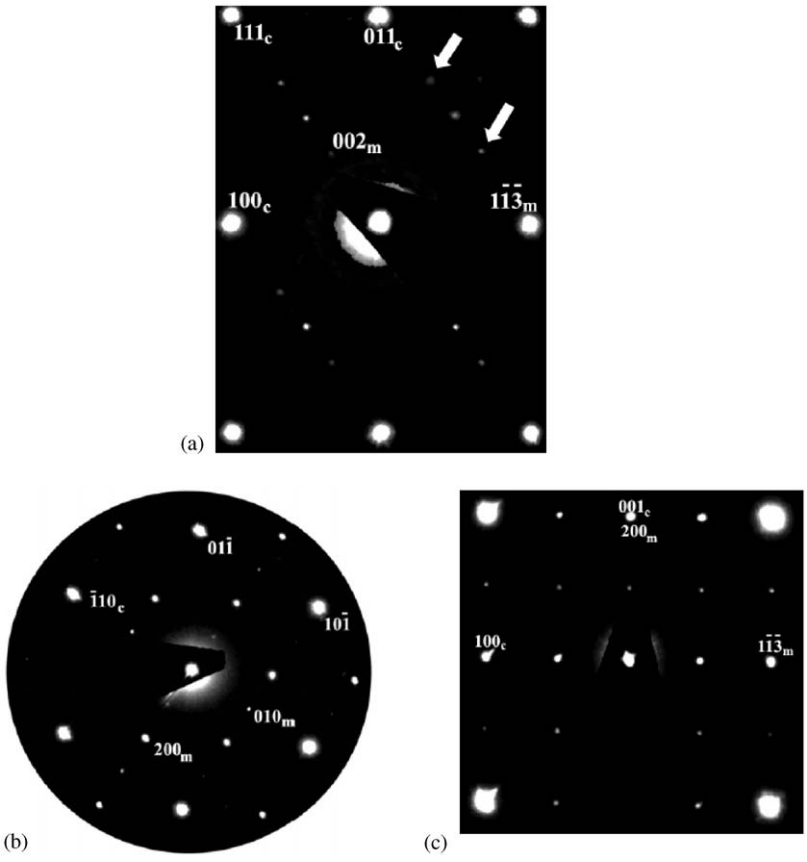

Fig. 2. Selected area diffraction patterns from 1:2 ordered $(1-x)Sr(Li_{1/4}Nb_{3/4})O_3$–$xSr(Li_{2/5}W_{3/5})O_3$ with $x = 0.333$ collected along: (a) $[0\bar{1}1]_c$, (b) $[111]_c$, and (c) $[010]_c$. Fundamental reflections are indexed in terms of the cubic sub-cell with a_c; superlattice reflections are indexed according to monoclinic unit cell with $a = \sqrt{6}a_c$, $b = \sqrt{2}a_c$, $c = 3\sqrt{2}a_c$, $\beta \approx 125°$.

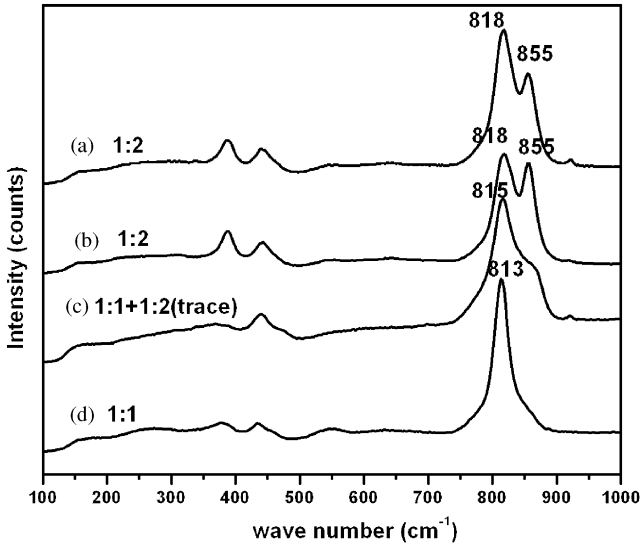

Fig. 3. Raman spectra of the powder specimens containing 1:2 ordered phase at $x = 0.238$ (a), and $x = 0.333$ (b), and 1:1 ordered structure at $x = 0.556$ (c), and $x = 0.833$ (d). The spectra of the 1:2 ordered phase are characterized by the splitting of peaks close to 815 and 855 cm^{-1}.

The final refined crystallographic parameters, atomic positions and displacement parameters, and atomic occupancies are listed in Tables 1 and 2 and the experimental, calculated and difference profiles are shown in Fig. 4. Alternate models for the cation distributions were investigated, e.g., a scheme with Li occupying B^{I}, Nb on B^{II}, and W distributed on both positions (W-distribution model). However, these led to higher reliability factors (see Table 3) and inferior agreement with bond valence calculations [23] (global instability index [24] = 0.235 compared to 0.173 for the Nb-distribution model).

The refined atomic occupancies were in good agreement with the Nb-distribution model for the non-stoichiometric 1:2 ordering with the majority of the Li cations (~81%) occupying the B^{I} site, all of the W cations on the B^{II} site, and Nb on both positions. The small degree of anti-site disorder reflected by the experimental occupancies could originate from localized disorder at ordering-induced domain boundaries that are typically present in these samples. Selected bond lengths (R) and the bond valence sums are summarized in Table 4 assuming 5+ and 6+ as the valence states for

Nb and W. Both of the crystallographically distinct B^{II} (Nb/W) octahedra are more distorted compared to the B^{II} (Li/Nb) octahedra. The resultant bond lengths are consistent with the refined structures of all the other known 1:2 *B*-site ordered perovskites, with the B^{II} cations undergoing a displacement from the center of their octahedra to lengthen the three B^{II}–O bonds in the B^{II}–O–B^{II} linkage (average bond length ~2.07 Å) and shorten the three bonds in a B^{II}–O–B^{I} linkage (average bond length ~1.92 Å). The refined structure is shown in Fig. 5, which also indicates the directions of the $b^-b^-c^+$ tilting. The structure obtained from the neutron refinement gave good agreement with the data collected using X-ray diffraction ($R_{wp} = 0.0730$, $R_p = 0.1021$, $R_F^2 = 0.0650$, Reduced $\chi^2 = 2.964$), which is shown in Fig. 6.

The dielectric properties of the samples exhibiting 1:2 order are listed in Table 5. All samples have dielectric

Table 1
Crystallographic data for neutron refinement of 1:2 ordered $(1-x)Sr(Li_{1/4}Nb_{3/4})O_3$–$xSr(Li_{2/5}W_{3/5})O_3$ at $x = 0.333$

Unit cell	$a = 9.7784(3)$ Å
(Space group $P2_1/c$, 14)	$b = 5.6463(2)$ Å
	$c = 16.9578(5)$ Å
	$\beta = 125.091(2)^\circ$
	Volume = 766.11(8) Å^3
R_p (profile)	0.0415
R_{wp} (weighted profile)	0.0500
R_F^2 (Bragg)	0.0498
Reduced χ^2	2.918
No. of structural parameters	86
Total no. of restraints	24
Contribution of restraints to χ^2	0.26%
Minimum 2θ	3
Maximum 2θ	165
No. of reflections	3299
Profile function	Pseudo-Voight (GSAS type 3)
Gaussian *U*, *V*, *W*	275, −252, 145
Cauchy *X*, *Y*	2.15, 1.34
Background function	Chebyschev polynomial (10 coefficients)

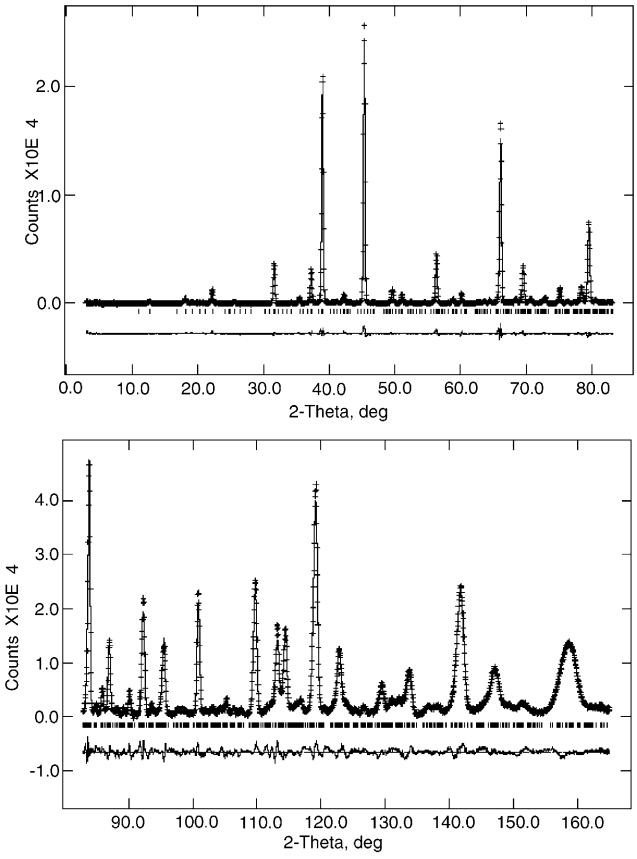

Fig. 4. Experimental (crosses), calculated (line), and difference profiles for neutron refinement of 1:2 ordered $(1-x)Sr(Li_{1/4}Nb_{3/4})O_3$–$xSr(Li_{2/5}W_{3/5})O_3$ at $x = 0.333$. The refinement parameters are given in Table 1.

Table 2
Refined structural parameters for 1:2 ordered $(1-x)Sr(Li_{1/4}Nb_{3/4})O_3$–$xSr(Li_{2/5}W_{3/5})O_3$ at $x = 0.333$

Atom	Site	Occupancy	*x*	*y*	*z*	$U \times 100$ Å^2
Sr1	4*e*	1.00	0.7411(1)	0.4893(2)	0.2465(1)	1.12(4)
Sr2	4*e*	1.00	0.2486(1)	0.5065(6)	0.0780(1)	1.20(7)
Sr3	4*e*	1.00	0.7496(1)	0.0173(1)	0.0890(5)	0.80(1)
Li/Nb1	2*a*	0.724(5)/0.276(2)	0	0	0	1.15(1)
Li/Nb2	2*d*	0.724(5)/0.276(2)	0.5	0.5	0	1.15(1)
Nb/W/Li3	4*e*	0.612(2)/0.30/0.088(5)	0.0109(1)	−0.0047(3)	0.3403(6)	0.82(7)
Nb/W/Li4	4*e*	0.612(2)/0.30/0.088(5)	0.4919	−0.0045(3)	0.1608(6)	0.82(7)
O1	4*e*	1.00	−0.0262(1)	0.2355(2)	0.0821(6)	1.32(3)
O2	4*e*	1.00	0.4739(1)	0.7161(2)	0.2283(6)	1.11(8)
O3	4*e*	1.00	−0.0089(1)	0.7576(2)	0.2413(5)	1.05(9)
O4	4*e*	1.00	0.5199(1)	0.2687(2)	0.1012(5)	1.14(1)
O5	4*e*	1.00	0.0313(1)	0.7628(2)	0.1046(6)	1.16(3)
O6	4*e*	1.00	0.4710(1)	0.7847(2)	0.0644(6)	0.93(1)
O7	4*e*	1.00	0.2520(2)	0.4508(2)	0.2461(8)	1.08(9)
O8	4*e*	1.00	0.7521(1)	0.5442(2)	0.0800(7)	1.06(2)
O9	4*e*	1.00	0.2560(2)	0.0403(2)	0.0893(7)	1.08(8)

constants close to 30, $Q \times f$ values between 20,000 and 30,000, and a negative temperature coefficient of the resonant frequency. While the microwave losses are comparable to several other perovskite oxides, they do not approach those of the stoichiometric 1:2 ordered $Ba(Zn_{1/3}Ta_{2/3})O_3$ systems.

Table 3
Reliability factors for different cation distribution models for 1:2 ordered $(1-x)Sr(Li_{1/4}Nb_{3/4})O_3$–$xSr(Li_{2/5}W_{3/5})O_3$, $x = 0.333$

	Nb-model $Sr[(Li_{3/4+y/2}Nb_{1/4-y/2})_{1/3}(Nb_{1-y}W_y)_{2/3}]O_3$	W-model $Sr[(Li_{4/5+2y/5}W_{1/5-2y/5})_{1/3}(Nb_{1-y}W_y)_{2/3}]O_3$
R_p (profile)	0.0415	0.0477
R_{wp} (weighted profile)	0.0500	0.0534
R_F^2 (Bragg)	0.0498	0.0519
Reduced χ^2	2.918	2.927

3.2. $(1-x)Ca(Li_{1/4}Nb_{3/4})O_3$–$(x)Ca(Li_{2/5}W_{3/5})O_3$ system

Single-phase 1:2 order was also observed in the $(1-x)Ca(Li_{1/4}Nb_{3/4})O_3$–$xCa(Li_{2/5}W_{3/5})O_3$ system within the range $0.238 \leqslant x \leqslant 0.333$ (Fig. 7). The lower tolerance factor of the Ca-based compositions ($t \sim 0.94$) increases the distortion of the perovskite cell and the associated peak splitting in the diffraction patterns becomes more pronounced. The patterns could be indexed using the $P2_1/c$ monoclinic cell, $a = 9.649(1)$ Å, $b = 5.427(3)$ Å, $c = 16.953(3)$ Å, $\beta = 125.55(2)^\circ$ for $x = 0.238$, and $a = 9.563(2)$ Å, $b = 5.335(2)$ Å, $c = 16.824(5)$ Å, $\beta = 125.28(3)^\circ$ for $x = 0.333$. Fig. 8 illustrates the agreement of the experimental diffraction pattern of $x = 0.238$ with a theoretical pattern calculated assuming 1:2 ordering of Li/Nb and Nb/W on the B^{I} and B^{II} sites and the positions obtained from the refinement of the corresponding SNLW phases.

A set of electron diffraction patterns obtained from an $x = 0.238$ specimen with well-developed $1/3[111]^*_c$

Table 4
Selected bond distances (R, Å) and bond valence sums (BVS, v.u.) for 1:2 ordered $(1-x)Sr(Li_{1/4}Nb_{3/4})O_3$–$xSr(Li_{2/5}W_{3/5})O_3$ at $x = 0.333$

B sites					
$(Li/Nb)_1$–O_1	$2.046(1) \times 2$	$(Li/Nb)_2$–O_4	$2.075(9) \times 2$		
$(Li/Nb)_1$–O_5	$2.100(1) \times 2$	$(Li/Nb)_2$–O_6	$2.052(1) \times 2$		
$(Li/Nb)_1$–O_9	$2.062(1) \times 2$	$(Li/Nb)_2$–O_8	$2.043(1) \times 2$		
Average	2.069	Average	2.057		
R_{max}/R_{min}	1.026	R_{max}/R_{min}	1.015		
BVS_{obs}	1.933	BVS_{obs}	1.997		
BVS_{cal}	2.103	BVS_{cal}	2.103		
$Nb_3/W_1/Li_3$–O_1	1.918(2)	$Nb_4/W_2/Li_4$–O_2	2.016(2)		
$Nb_3/W_1/Li_3$–O_3	2.069(2)	$Nb_4/W_2/Li_4$–O_2	2.116(2)		
$Nb_3/W_1/Li_3$–O_3	2.021(2)	$Nb_4/W_2/Li_4$–O_4	1.947(2)		
$Nb_3/W_1/Li_3$–O_5	1.940(2)	$Nb_4/W_2/Li_4$–O_6	1.935(1)		
$Nb_3/W_1/Li_3$–O_7	2.119(2)	$Nb_4/W_2/Li_4$–O_7	2.069(2)		
$Nb_3/W_1/Li_3$–O_8	1.916(2)	$Nb_4/W_2/Li_4$–O_9	1.907(2)		
Average	1.997	Average	1.998		
R_{max}/R_{min}	1.106	R_{max}/R_{min}	1.110		
BVS_{obs}	4.585	BVS_{obs}	4.562		
BVS_{cal}	4.948	BVS_{cal}	4.948		
A sites					
Sr_1–O_1	2.973(1)	Sr_2–O_1	3.128(1)	Sr_3–O_1	2.575(1)
Sr_1–O_2	2.762(1)	Sr_2–O_1	2.727(1)	Sr_3–O_3	2.717(1)
Sr_1–O_2	2.831(2)	Sr_2–O_2	2.509(1)	Sr_3–O_3	2.857(1)
Sr_1–O_3	2.920(1)	Sr_2–O_2	3.255(1)	Sr_3–O_4	2.763(1)
Sr_1–O_3	2.827(1)	Sr_2–O_4	2.792(2)	Sr_3–O_4	3.192(1)
Sr_1–O_4	2.484(1)	Sr_2–O_5	2.814(2)	Sr_3–O_5	2.981(1)
Sr_1–O_5	2.550(1)	Sr_2–O_5	3.106(1)	Sr_3–O_6	2.831(2)
Sr_1–O_6	3.149(1)	Sr_2–O_6	2.798(2)	Sr_3–O_6	2.494(1)
Sr_1–O_7	3.043(1)	Sr_2–O_7	2.849(1)	Sr_3–O_7	2.830(2)
Sr_1–O_7	2.607(1)	Sr_2–O_8	2.690(1)	Sr_3–O_8	2.676(1)
Sr_1–O_8	2.904(1)	Sr_2–O_9	2.637(1)	Sr_3–O_8	2.980(1)
Sr_1–O_9	2.783(1)	Sr_2–O_9	3.018(1)	Sr_3–O_9	3.010(1)
Average	2.819	Average	2.860	Average	2.826
BVS_{obs}	2.06	BVS_{obs}	1.88	BVS_{obs}	2.01
BVS_{cal}	2.00	BVS_{cal}	2.00	BVS_{cal}	2.00

reflections is shown in Fig. 9, and indexed with respect to the cubic perovskite sub-cell and the monoclinic supercell ($a_m = [\bar{1}\bar{1}2]_c$, $b_m = [1\bar{1}0]_c$, $c_m = 3[110]_c$). Again reflections from the $1/2[111]_c^*$ and $1/2[1\bar{1}0]_c^*$-type satellites and the $1/3[111]_c^*$ ordering reflections provide direct evidence that the $b^-b^-c^+$ type octahedral tilting accompanies the 1:2 order. The electron diffraction patterns for these phases are almost identical to those previously reported for 1:2 ordered $Ca_4Nb_2O_9$ [20], which has a similar tolerance factor and resultant distorted structure.

Single-phase perovskites could not be formed for $x > 0.333$ where a variety of non-perovskite calcium tungstates dominated the X-ray powder patterns. For

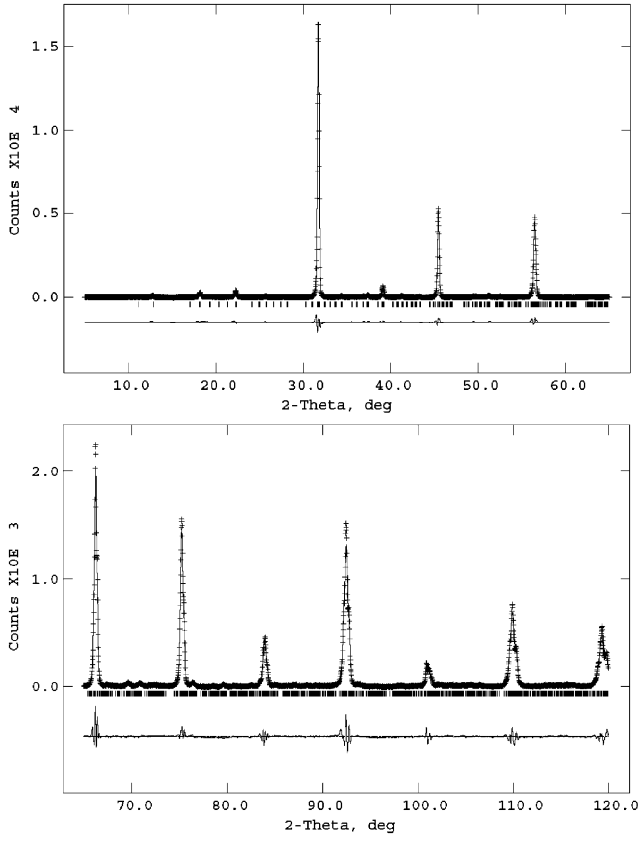

Fig. 5. Experimental (crosses) and calculated (line) powder X-ray diffraction profiles of the 1:2 ordered structure at composition $x = 0.333$. The calculated profile used the final parameters of the neutron refinement.

Table 5
Microwave dielectric properties of $(1-x)Sr(Li_{1/4}Nb_{3/4})O_3$–$(x)Sr(Li_{2/5}W_{3/5})O_3$

x	Bulk density (%)	f (GHz)	Qf (GHz)	ε	τ_f (ppm/°C)
0.283	94	9.10	23,800	28	−29
0.333	96	8.71	27,400	31	−23
0.385	93	9.15	21,200	30	−33

Note: ε values are corrected to theoretical density.

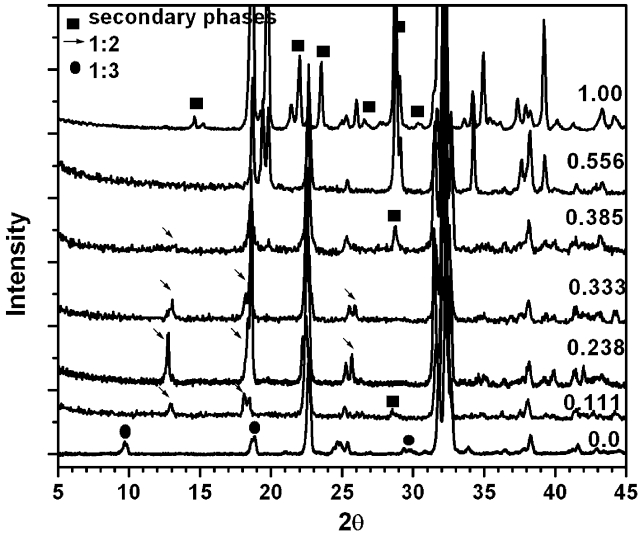

Fig. 7. XRD patterns of $(1-x)Ca(Li_{1/4}Nb_{3/4})O_3$–$xCa(Li_{2/5}W_{3/5})O_3$ with $x = 1.00$, 0.556, 0.385, 0.333, 0.238, 0.111, and 0.0. All samples were equilibrated at 1100–1150 °C for 5–10 h. Arrows indicate reflections associated with 1:2 order, circles 1:3 order, and squares secondary phases.

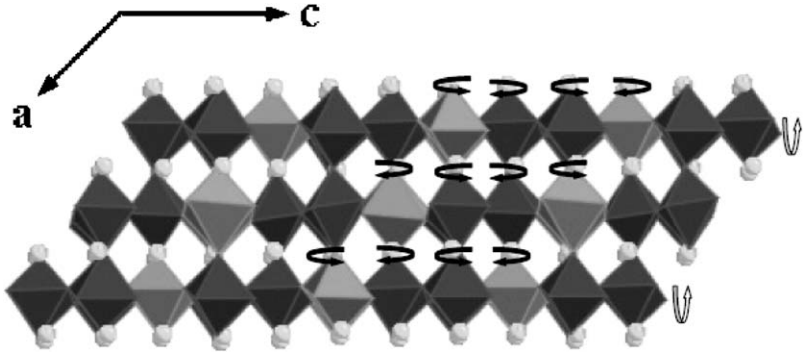

Fig. 6. Schematic illustration of the 1:2 ordered structure for $(1-x)Sr(Li_{1/4}Nb_{3/4})O_3$–$xSr(Li_{2/5}W_{3/5})O_3$. Spheres represent A-site Sr cations, black polyhedra represent B^{II}-sites preferentially occupied by W and Nb, light polyhedra B^{I}-sites occupied by Li and Nb. Arrows indicate directions of octahedral rotation.

$x<0.238$ the patterns contained peaks from the $Ca(Li_{1/4}Nb_{3/4})O_3$ end member, which has a 1:3 ordered arrangement of Li and Nb ($x=0$ in Fig. 7) and the 1:2 ordered phase [16].

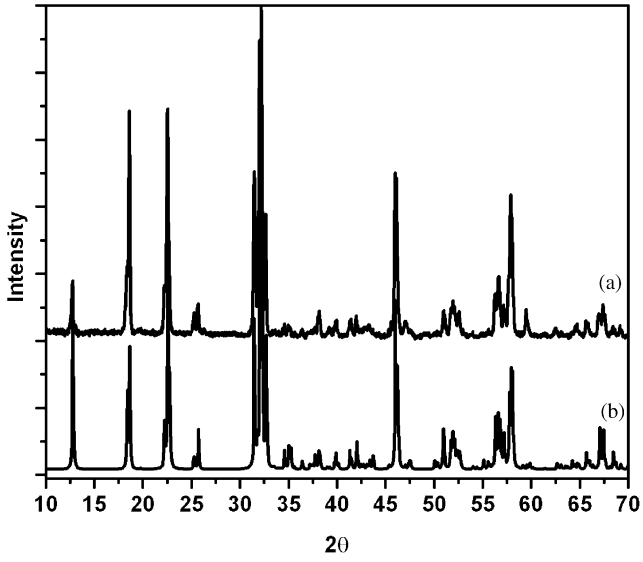

Fig. 8. Observed (a), and calculated (b) patterns for 1:2 ordered structure of $(1-x)Ca(Li_{1/4}Nb_{3/4})O_3$–$xCa(Li_{2/5}W_{3/5})O_3$ at $x=0.238$.

The 1:2 ordered CNLW perovskites could be sintered to high density (>94%) at quite low temperatures (1100–1150 °C). An SEM micrograph of the thermally etched surface of a sintered pellet of $x=0.333$, with grain sizes in the range 1–3 μm, is shown in Fig. 10. The dielectric properties of the sintered ceramics measured at

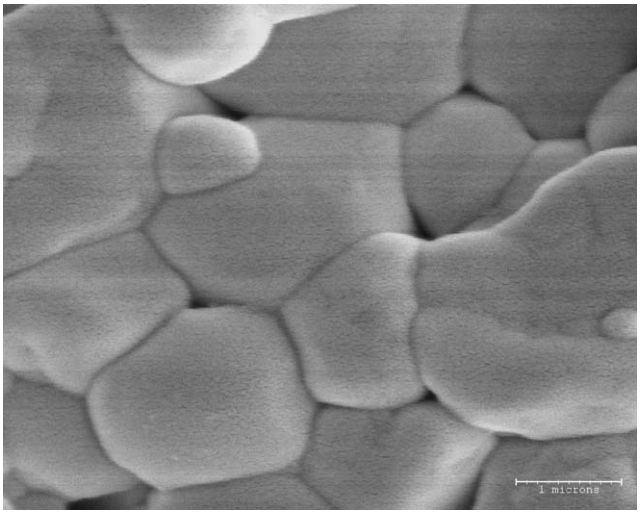

Fig. 10. SEM micrograph of a dense sample of 1:2 ordered perovskite in $(1-x)Ca(Li_{1/4}Nb_{3/4})O_3$–$xCa(Li_{2/5}W_{3/5})O_3$ ($x=0.238$) after sintering at 1150 °C for 10 h.

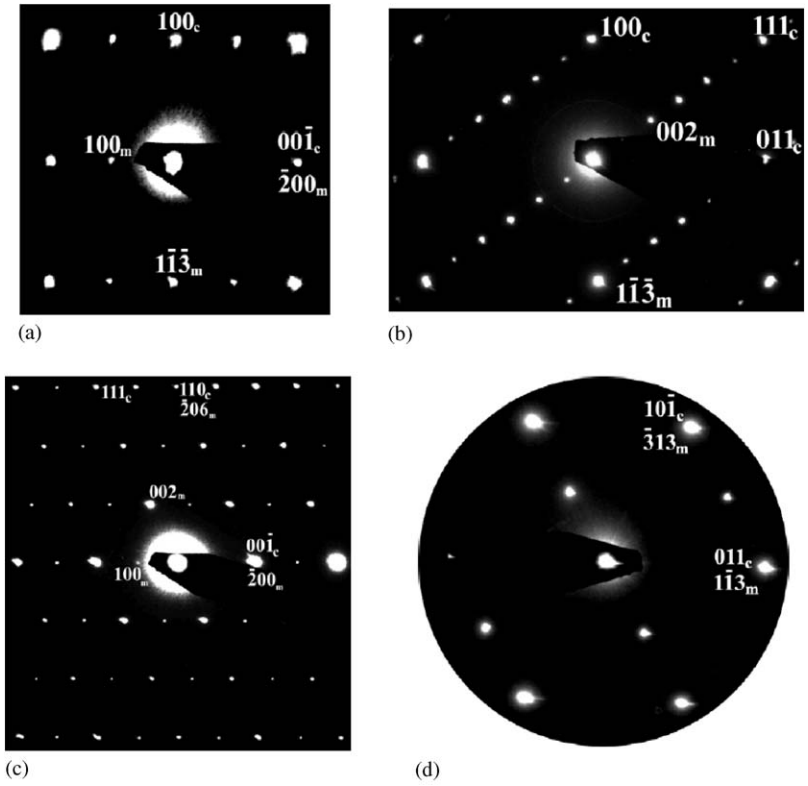

Fig. 9. Selected area diffraction patterns from 1:2 ordered $(1-x)Ca(Li_{1/4}Nb_{3/4})O_3$–$xCa(Li_{2/5}W_{3/5})O_3$ with $x=0.238$ collected along: (a) $[010]_c$, (b) $[01\bar{1}]_c$, (c) $[\bar{1}10]_c$, and (d) $[\bar{1}1\bar{1}]_c$. Fundamental reflections indexed in terms of the cubic sub-cell with a_c; superlattice reflections according to monoclinic unit cell with $a=\sqrt{6}a_c$, $b=\sqrt{2}a_c$, $c=3\sqrt{2}a_c$, and $\beta\approx125°$.

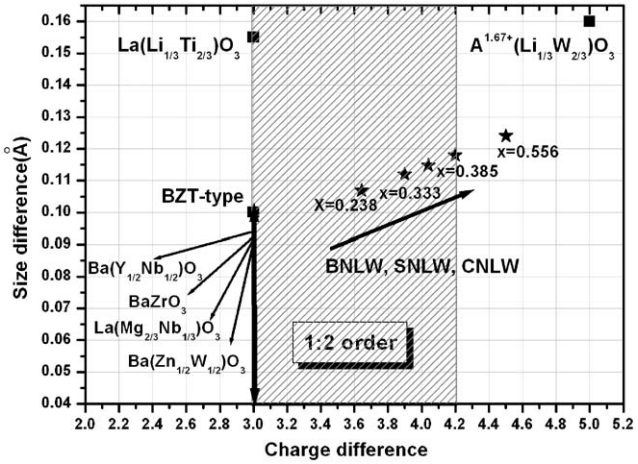

Fig. 11. Schematic illustration of the effect of size and charge differences on the stabilization of 1:2 *B*-site order in oxide perovskites. Hatched area represents observed region of stability for 1:2 order; unshaded areas with lower and higher charge differences represent fields of stability for alternate *B*-site order (1:1 type or disordered) or formation of non-perovskites phases (e.g., $A^{1.67+}(Li_{1/3}W_{2/3})O_3$. Stars represent compositions of $(1-x)A(Li_{1/4}Nb_{3/4})O_3$–$xA(Li_{2/5}W_{3/5})O_3$; solid solutions ($A$ = Ba = BNLW, = Sr = SNLW, = Ca = CNLW). Lines represent changes in charge/size for solid solutions of $Ba(Zn_{1/3}Ta_{2/3})O_3$ (BZT) with the indicated end members.

microwave frequencies were: $x = 0.238$, $\varepsilon = 31$, $Q \times f = 22720$ at 10.29 GHz, $\tau_f = -33$ ppm/°C; $x = 0.333$, $\varepsilon = 29$, $Q \times f = 15690$ at 9.66 GHz, $\tau_f = -35$ ppm/°C.

4. Discussion

Investigation of the phase relations in $(1-x)Sr(Li_{1/4}Nb_{3/4})O_3$–$(x)Sr(Li_{2/5}W_{3/5})O_3$ and $(1-x)Ca(Li_{1/4}Nb_{3/4})O_3$–$(x)Ca(Li_{2/5}W_{3/5})O_3$ showed that non-stoichiometric 1:2 *B*-site ordered perovskites are stable in both systems. Rietveld refinements of the SNLW system were consistent with the models previously advanced to describe the cation distribution in the corresponding $(1-x)Ba(Li_{1/4}Nb_{3/4})O_3$–$(x)Ba(Li_{2/5}W_{3/5})O_3$ system, with the B^{I} positions in the $A(B^{I}_{1/3}B^{II}_{2/3})O_3$ structure preferentially occupied by Li, the B^{II} positions by W, and the Nb cations distributed over both positions according to the general stoichiometry: $A^{2+}[(Li_{3/4+y/2}Nb_{1/4-y/2})_{1/3}(Nb_{1-y}W_y)_{2/3}]O_3$, ($y = 0.9x$). Although the observation of 1:2 cation order in these systems is very similar to that reported for the BNLW system, the symmetry of the ordered structure is lowered from trigonal $P\bar{3}m1$ to monoclinic $P2_1/c$ through the occurrence of $b^-b^-c^+$-type octahedral tilting, and the range of homogeneity for the order is slightly narrower ($0.238 \leqslant x \leqslant 0.333$ for SNLW and CNLW compared to $0.238 \leqslant x \leqslant 0.385$ for BNLW).

Because the 1:2 ordered CNLW and SNLW phases are so similar to their BNLW counterparts, their formation and range of stability can be rationalized using the same crystal chemical arguments. For BNLW, the stabilization of non-stoichiometric 1:2 order was explained in terms of the large difference in the charge (Δq) of the B^{I} and B^{II} positions that results from the ordering of Li and W. For SNLW and CNLW single phase 1:2 order first appears at $x = 0.238$ ($y = 0.214$), where $\Delta q = +3.64$, and is retained up to $x = 0.333$ ($y = 0.30$) where $\Delta q = +3.9$. The increase in Δq with y is accompanied by an increase in the B^{I}/B^{II} size difference. The loss of the 1:2 order in favor of 1:3-type ordered arrangements for $y \leqslant 0.21$ is presumably associated with the high charge/size mismatch of the Li/Nb ions on the B^{I} site, which increases as y decreases. However, the absence of 1:2 order in solid solutions with $0.30 < y \leqslant 0.5$, which would have the highest charge/size site differences and the lowest on-site mismatches, cannot be rationalized by these arguments. For the BNLW system we noted the loss of 1:2 order for the W-rich solid solutions could arise from imbalances in the local anion bond valences due to the formation of W–O–W linkages, but proposed the destabilization was more likely a result of the incompatibility of the *B*-site distributions with the local charges on the *A*-site lattice [15]. In this structure, the $\{\ldots B^{I}B^{II}B^{II}\ldots\}$ layering creates two different *A*-site environments: the A^{I} site (Sr1 in Table 2) is located between two B^{II} layers and has six B^{II} and two B^{I} nearest neighbors; the two A^{II} sites (Sr2 and Sr3) are located between a B^{I} and a B^{II} layer and have five B^{II} and three B^{I} nearest neighbors. For tungsten-rich compositions such as $Sr[Li_{1/3}(Nb_{1/2}W_{1/2})_{2/3}]O_3$ the B^{II} charge of 5.5^+ would give a formal framework charge = −1.625 and −2.1875 in the A^{I} and A^{II} sub-cells and resultant formal ionic charge mismatches = 0.375 and −0.1875, respectively. The random occupancy of B^{II} by Nb and W would give a distribution of environments with much higher local imbalances that could range from $\Delta q = +0.75$ to 0.0 at A^{I}, and +0.125 to –0.5 at A^{II} for environments with Nb:W = 0:6 and 6:0, respectively. We believe these large mismatches at the higher W concentrations are responsible for the loss of 1:2 order.

In the SNLW and CNLW systems, the range of single phase 1:2 order is slightly narrower compared to the BNLW system. This is unusual as typically the stability of an ordered phase with a specific *B*-site chemistry is increased by a lower tolerance factor; e.g., $Sr(Zn_{1/3}Nb_{2/3})O_3$ retains a 1:2 ordered structure to very high temperatures, while $Ba(Zn_{1/3}Nb_{2/3})O_3$ undergoes a disordering transition at ~1375 °C. It is possible that the narrower range of stability reflects the importance of the local formal charge imbalance at the *A*-sites which would be expected to play a larger role as the overall volume of the cell is reduced, as is the case for the Ca and Sr systems.

As noted earlier, in the $Ba(Zn_{1/3}Ta_{2/3})O_3$ family of perovskites very low levels of a substituent (e.g., ⩽3%

$BaZrO_3$ or $\leqslant 0.5\%$ $Ba(Zn_{1/2}W_{1/2}O_3)$ of different size/charge on the B^{I} or B^{II} sites induce a transition to a 1:1 ordered non-stoichiometric structure [4,8–14]. However, the SNLW, CNLW, and BNLW 1:2 ordered phases clearly tolerate extensive non-stoichiometry. In Fig. 11, the known 1:2 ordered perovskite systems are mapped as a function of the charge and size difference of the B^{I} and B^{II} sites. For the BZT-type $Ba(B^{2+}_{1/3}B^{5+}_{2/3})O_3$ systems the charge difference (Δq) = 3, and the size difference (Δr) ranges from 0.05 Å (Ni) to much higher values in $Ba(Sr_{1/3}Ta_{2/3})O_3$($\Delta r = 0.54$ Å). Two other recently reported stoichiometric 1:2 ordered perovskites, $La(Li_{1/3}Ti_{2/3})O_3$ and $(Sr_{2/3}La_{1/3})[Li_{1/3}(Ta, Nb)_{2/3}]O_3$ have $\Delta q = 3$ and 4, and $\Delta r = 0.155$ and 0.12 Å, respectively. The only other known stoichiometric 1:2 ordered phase, $Ba(Bi_{2/3}Te_{1/3})O_3$ [25] also has a charge difference of 3 and a large size difference ($r = 0.47$ Å). No 1:2 ordered systems have been reported with $\Delta q < 3.0$. For all the different additives that destabilize the order in BZT, the substitutions would reduce the charge difference to a value below 3.0 (e.g., $BaZrO_3$, $Ba(Zn_{1-x}Zr_x)_{1/3}(Ta_{1-x}Zr_x)_{2/3}O_3$; $LaZn_{2/3}Ta_{1/3}O_3$, $Ba_{1-x}La_x(Zn)_{1/3}(Ta_{1-x/2}Zn_{x/2})_{2/3}O_3$), or increase the on-site charge mismatch without increasing Δq or Δr (e.g., $BaZn_{1/2}W_{1/2}O_3$, $Ba(Zn)_{1/3}(Ta_{1-x}W_{3x/4}Zn_{x/4})_{2/3}O_3$). The stable 1:2 phases in the BLNW/SNLW/CNLW systems all have Δq's $> +3.6$ which suggests that non-stoichiometry can only be sustained when the substituents increase the site charge difference to a value greater than 3. However, for W-rich compositions with Δq's close to 4.5 (e.g., $(Sr,Ca)[Li_{1/3}(Nb_{1/2}W_{1/2})_{2/3}]O_3$), or even higher (e.g., $A^{5/3+}(Li_{1/3}W_{2/3})O_3$ [15]), the stability of the order is apparently mediated by local charge imbalances at the A-sites. This stability field map would suggest that non-stoichiometric 1:2 perovskites should be stable in other systems where values of $\Delta q \geqslant 3.0$ can be realized. For example, the partial substitution of W into phases such as $(Sr_{2/3}La_{1/3})(Li_{1/3}Nb_{2/3})O_3$ through the formation of $(Sr_{2+x/3}La_{1-x/3})[Li_{1/3}(Nb_{1-x}W_x)_{2/3}]O_3$ solid solutions would yield $\Delta q > 4.0$ and should exhibit stable 1:2 order. Investigations of these solid solutions are currently in progress.

Finally, we note that the $(1-x)$ $Sr(Li_{1/4}Nb_{3/4})O_3$–$(x)Sr(Li_{2/5}W_{3/5})O_3$ is the only system that exhibits all three types of B-site order (1:1, 1:2 and 1:3). The 1:3 order is restricted to a narrow range close to the $Sr(Li_{1/4}Nb_{3/4})O_3$ end member; 1:1 order is observed from $x = 0.833$, $Sr(Li_{3/4}Nb_{1/4})_{1/2}(W)_{1/2}O_3$, up to $x = 1$, $Sr(Li_{4/5}W_{1/5})_{1/2}(W)_{1/2}O_3$, with the complete avoidance of Li and W in the former being accompanied by the strongest superlattice reflections.

5. Conclusions

Non-stoichiometric 1:2 ordered phases in the $(1-x)A^{2+}(Li_{1/4}Nb_{3/4})O_3$–$(x)A^{2+}(Li_{2/5}W_{3/5})O_3$, ($A^{2+}$ = Sr and Ca), solid solution systems were identified in the range of $0.238 \leqslant x \leqslant 0.333$. Similar to their Ba analogs, the ordered SLNW and CLNW solid solutions do not include any composition with a 1:2 cation stoichiometry and the two sites in the structure exhibit extensive non-stoichiometry ($A^{2+}[(Li_{3/4+y/2}Nb_{1/4-y/2})_{1/3}(Nb_{1-y}W_y)_{2/3}]O_3$, $y = 0.21-0.30$, where $y = 0.9x$). Qualitative analysis of X-ray powder diffraction and selected area electron diffraction data revealed that the 1:2 non-stoichiometric ordering is combined with $b^-b^-c^+$ octahedral tilting and the structure can be described by a monoclinic $P2_1/c$ supercell with lattice parameters $a = \sqrt{6}a_c$, $b = \sqrt{2}a_c$, $c = 3\sqrt{2}a_c$, $\beta \approx 125^\circ$. This model of the ordered structure and the site occupancies was validated and supported by Rietveld refinement using neutron diffraction. The stability of the 1:2 ordered structure is affected by the charge/size differences of the two B-sites, the over-bonding of the anions in W–O–W linkages, and the local charge imbalances at the A-sites. For the Sr system, a 1:3 ordered phase was observed at $x = 0.111$ and is similar to the high-temperature 1:3 ordered polymorph reported for the $x = 0.0$ end member, and 1:1 ordered phases were observed for $0.833 \leqslant x \leqslant 1.0$. For the Ca solid solutions, non-perovskite phases are formed for $0.333 < x \leqslant 1.0$. The 1:2 ordered ceramic specimens exhibit quite good quality factors and negative temperature coefficients of the resonant frequency in the microwave region.

Acknowledgments

This work was supported by the National Science Foundation (Grant No. DMR 02-13489) and made use of the MRSEC shared experimental facilities supported by the National Science Foundation through Grant No. DMR 00-79909. We thank Dr. Igor Levin and Dr. Brian Toby at NIST for assistance with the neutron data collection. We also acknowledge the support of the National Institute of Standards and Technology, US Department of Commerce, in providing the neutron research facilities used in this work.

References

[1] S. Kawashima, M. Nishida, I. Ueda, H. Ouchi, J. Am. Ceram. Soc. 66 (6) (1983) 421–423.
[2] K. Matsumoto, T. Hiuga, K. Takada, H. Ichimura, in: Proceedings of the Sixth IEEE International Symposium on Application of Ferroelectrics (June 1986), Institute of Electrical and Electronic Engineers, New York, 1986, pp. 118–121.
[3] H. Tamura, T. Konoike, Y. Sakabe, K. Wakina, J. Am. Ceram. Soc. 67 (4) (1984) C-59–C-61.
[4] P.K. Davies, J. Tong, T. Negas, J. Am. Ceram. Soc. 80 (7) (1997) 1727–1740.
[5] A.Y. Borisevich, P.K. Davies, J. Solid State Chem. 170 (2003) 198–201.

[6] P.K. Davies, A. Borisevich, M. Thirumal, J. Eur. Ceram. Soc. 23 (2003) 2461–2466.
[7] A.Y. Borisevich, P.K. Davies, Appl. Phys. Lett. 84 (8) (2004) 1347–1349.
[8] L. Chai, P.K. Davies, J. Am. Ceram. Soc. 80 (12) (1997) 3193–3198.
[9] L. Chai, M.A. Akbas, P.K. Davies, J.B. Parise, Mater. Res. Bull. 32 (9) (1997) 1261–1269.
[10] M.A. Akbas, P.K. Davies, J. Am. Ceram. Soc. 81 (8) (1998) 2205–2208.
[11] M.A. Akbas, P.K. Davies, J. Am. Ceram. Soc. 81 (3) (1998) 670–676.
[12] M.A. Akbas, P.K. Davies, J. Am. Ceram. Soc. 81 (4) (1998) 1061–1064.
[13] I. Molodetsky, P.K. Davies, J. Euro. Ceram. Soc. 21 (2001) 2587–2591.
[14] B. Jancar, P.K. Davies, D. Suvorov, M. Valant, Inst. Jozef Stefan, Ljubljana, Slovenia, in: P. Glavic, D. Brodnjak-Voncina (Eds.), Zbornik Referatov s Posvetovanja Slovenski Kemijski Dnevi, Maribor, Slovenia, September 26–27 (Part 2), Univerza v Mariboru, Fakulteta za Kemijo in Kemijsko Tehnologijo, Maribor, Slovenia, 2002, pp. 808–813.
[15] H. Wu, P.K. Davies, J. Solid State Chem. 177 (2004) 3469–3478.
[16] A. Borisevich, Investigation of Li-containing dielectric oxides for microwave applications, Ph.D. Dissertation, University of Pennsylvania, 2002.
[17] Y. Hikichi, Z. Chen, R.E. Newnham, L.E. Cross, Mater. Res. Bull. 17 (1982) 1371–1377.
[18] Y. Hikichi, S. Suzuki, J. Am. Ceram. Soc. 70 (5) (1987) C-99–C-100.
[19] A.C. Larson, R.B. Von Dreele, General Structure Analysis System, Report LAUR 86-748, Los Alamos National Laboratory, NM, 1994.
[20] I. Levin, L.A. Bendersky, J.P. Cline, R.S. Roth, T.A. Vanderah, J. Solid State Chem. 150 (2000) 43–61.
[21] I. Levin, J.Y. Chan, R.G. Geyer, J.E. Maslar, T.A. Vanderah, J. Solid State Chem. 156 (2001) 122–134.
[22] G. Blasse, A.F. Corsmit, J. Solid State Chem. 10 (1974) 39–45.
[23] I.D. Brown, D. Altermatt, Acta Crystallogr. B 41 (1985) 244–247.
[24] M.W. Lufaso, P.M. Woodward, Acta Crystallogr. B 57 (2001) 725–738.
[25] J.–H. Park, P.M. Woodward, Int. J. Inorg. Mater. 2 (1) (2000) 153–166.